

AN INVESTIGATION OF THE PROCESSES $e^+e^- \rightarrow \mu^+\mu^-\gamma$ AND $e^+e^- \rightarrow e^+e^-\gamma$

CELLO Collaboration

H.-J. BEHREND, J. BÜRGER, L. CRIEGEE, H. FENNER, J.H. FIELD, G. FRANKE,
J. MEYER, V. SCHRÖDER, H. SINDT, U. TIMM, G.G. WINTER, W. ZIMMERMANN*Deutsches Elektronen-Synchrotron, DESY, D-2000 Hamburg 52, Germany*P.J. BUSSEY, A.J. CAMPBELL, J.B. DAINTON, D. HENDRY, G. McCURRACH, J.M. SCARR,
I.O. SKILLICORN, K.M. SMITH*University of Glasgow, Glasgow G12 8QQ, United Kingdom*

V. BLOBEL, M. POPPE, H. SPITZER

*II. Institut für Experimentalphysik, Universität Hamburg, D-2000 Hamburg 50, Germany*W.-D. APEL, J. ENGLER, G. FLÜGGE, D.C. FRIES, W. FUES, K. GAMERDINGER,
P. GROSSE-WIESMANN, J. HANSMEYER, Th. HENKES, G. HOPP, H. JUNG, J. KNAPP,
M. KRÜGER, H. KÜSTER, H. MÜLLER, K.H. RANITZSCH, H. SCHNEIDER*Kernforschungszentrum Karlsruhe and Universität Karlsruhe, D-7500 Karlsruhe, Germany*W. DE BOER, G. BUSCHHORN, W. CHRISTIANSEN, B. FATAH, G. GRINDHAMMER,
B. GUNDERSON, Ch. KIESLING, R. KOTTHAUS, H. KROHA, D. LÜERS, H. OBERLACK,
P. SCHACHT, B. SCHARLEMANN, G. SHOOSHTARI, W. WIEDENMANN*Max-Planck-Institut für Physik und Astrophysik, D-8000 Munich 40, Germany*A. CORDIER, M. DAVIER, D. FOURNIER, M. GAILLARD, J.F. GRIVAZ, J. HAISSINSKI,
V. JOURNÉ, F. LE DIBERDER, E. ROS, A. SPADAFORA, J.-J. VEILLET*Laboratoire de l'Accélérateur Linéaire, F-94405 Orsay Cedex, France*R. GEORGE, M. GOLDBERG, O. HAMON, F. KAPUSTA, F. KOVACS, R. PAIN,
L. POGGIOLI, M. RIVOAL*Laboratoire de Physique Nucléaire et Hautes Energies, Université de Paris, F-91405 Orsay Cedex, France*

G. D'AGOSTINI, M. GASPERO, B. STELLA

*University of Rome and INFN, I-00185 Rome, Italy*R. ALEKSAN, G. COZZIKA, Y. DUCROS, P. JARRY, Y. LAVAGNE, F. OULD SAADA,
J. PAMELA, F. PIERRE*Centre d'Etudes Nucléaires, Saclay, F-91191 Gif-sur-Yvette Cedex, France*

G. ALEXANDER, G. BELLA, Y. GNAT and J. GRUNHAUS

Tel Aviv University, Ramat Aviv, Tel Aviv 69978, Israel

Received 18 October 1984; revised manuscript received 15 May 1985

The reactions $e^+e^- \rightarrow \mu^+\mu^-\gamma$ and $e^+e^- \rightarrow e^+e^-\gamma$ have been studied with the CELLO detector at the PETRA storage ring. Data have been collected from $\sqrt{s} = 14$ GeV up to 46.8 GeV. In a Dalitz plot analysis of the data, good agreement is found with QED, except for the region $M_{\mu\gamma}^2 > 0.8$ where the probability that QED describes the high energy data is at the percent level.

Introduction. In this letter, we report on a study of the reactions

$$e^+e^- \rightarrow \mu^+\mu^-\gamma, \quad (1)$$

$$e^+e^- \rightarrow e^+e^-\gamma. \quad (2)$$

The data were obtained using the CELLO detector operating at the PETRA storage ring at DESY. These reactions should be well described by QED calculations [1–4] of order α^3 . Data have been collected over a wide energy range, from $\sqrt{s} = 14$ GeV to 46.8 GeV, the maximum centre of mass energy reached by PETRA. Results for reaction (1) based on part of our present data have been communicated previously [5].

Detector properties and event selection. The main features of the CELLO detector [6] used in this analysis are its good resolution and its large and uniform detection coverage for charged particles and photons. Charged particles are detected and analyzed in the angular range $11^\circ < \theta < 169^\circ$ with a momentum resolution $\Delta p/p^2 = 2 \times 10^{-2}$ (p in GeV/ c) and angular resolutions $\sigma_\theta = 3 \text{ mr} \cdot \sin^2\theta$ and $\sigma_\phi = 2 \text{ mr}$ in the central region $30^\circ < \theta < 150^\circ$ and progressive loss of accuracy outside. Electromagnetic calorimetry is realized with a lead–liquid argon system in which granularity has been optimized both transversely and longitudinally, enabling a good angular resolution and a satisfactory hadron–muon/electron separation to be achieved. The photon angular resolutions are: $\sigma_\theta = (10 \pm 2) \text{ mr}$ and $\sigma_\phi = (6 \pm 1) \text{ mr}$. The photon energy resolution is $\sigma_E/E = 5\% + 10\%/\sqrt{E}$ with E in GeV. The calorimeter covers 96% of the solid angle. Muons can be separated from electrons and hadrons by their characteristic minimum-ionizing behaviour in the calorimeter and their penetration through 80 cm of iron followed by detection in wire chambers covering 92% of the solid angle. The minimum momentum for μ detection in the muon chambers is 1.4 GeV/ c . The detector is triggered by combinations of charged tracks and energy

deposition. Reactions (1) and (2) were recorded by two independent triggers: one requiring two charged tracks, the other requiring a single track and an energy deposition in liquid argon greater than 2 GeV. In addition, reaction (2) was recorded using a purely calorimetric trigger. It was therefore possible to cross-check the triggers involved for reactions (1) and (2) and achieve an overall trigger efficiency of $\approx 95\%$ for reaction (1) and greater than 99% for reaction (2) within the detection solid angle described below.

The event candidates were selected with the following criteria:

- (i) Two and only two tracks with $|\cos \theta| < 0.85$ with a momentum larger than $0.05 E_{\text{beam}}$. In addition, the acoplanarity angle was required to be between 2° and 178° .
- (ii) One photon shower with $|\cos \theta| < 0.85$ and energy larger than $0.10 E_{\text{beam}}$: no other significant (> 0.5 GeV) shower in the calorimeter was allowed.
- (iii) A minimum angle of 10° between the photon and lepton directions to avoid collinear radiation and confusion with $\tau\tau$ events where a $\pi\pi^0$ final state could simulate the $\mu\gamma$ topology.
- (iv) A minimum visible energy of $0.6\sqrt{s}$ to eliminate remaining $\tau\tau\gamma$ events.
- (v) A minimum value of $0.05\sqrt{s}$ for the ee or $\mu\mu$ mass in order to avoid the contamination of events with a $\gamma\rho^0$ final state.

Muons were identified by their energy deposition in the 1.1 absorption length-deep calorimeter or a hit recorded in the chambers surrounding the iron absorber: the distribution of energy deposited in the calorimeter for the final sample is given in fig. 1a. The ratio of the distance between the impact of the extrapolated track in the muon chamber and the recorded hit to the estimated position uncertainty is shown in fig. 1b. 77% of the tracks in reaction (1) are positively identified by the muon chambers and 85% are reconstructed as minimum ionizing particles in the lead–liquid argon calorimeter. These values are in accor-

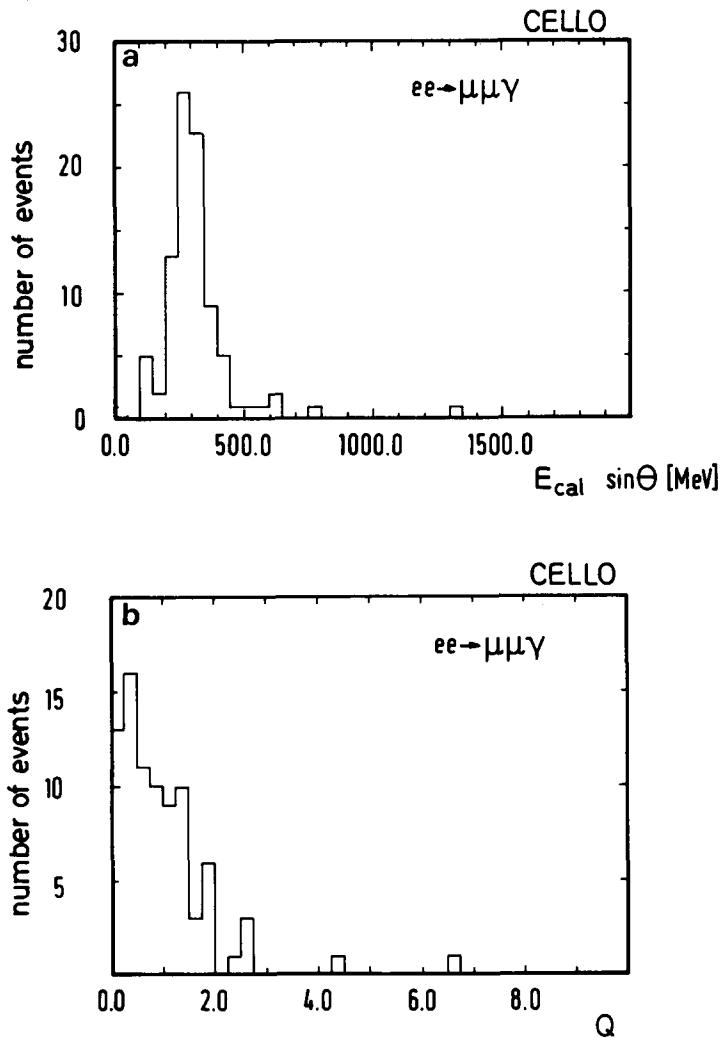


Fig. 1. (a) The energy deposition of the tracks in the lead-liquid argon calorimeter. (b) The ratio (Q) of the distance between the extrapolated impact of a track in the muon chamber and the recorded hit to the estimated position uncertainty.

dance with the acceptance (dead areas, momentum cutoff) and the known inefficiencies of these devices. As a check, all the candidates were visually scanned before applying the identification cuts.

Table 1 shows the data sample obtained at the different centre of mass energies.

Kinematic reconstruction. The complete measurement of reactions (1) and (2) is kinematically over-constrained (4C). However angular measurements are more precise in our detector than energy measure-

Table 1
Data sample for the process $ee \rightarrow \mu\mu\gamma$ and $ee \rightarrow ee\gamma$ within the cuts described in the text.

CM energy [GeV]	Integrated luminosity [pb^{-1}]	$ee \rightarrow \mu\mu\gamma$ number of events	$ee \rightarrow ee\gamma$ number of events
14	0.6	8	119
22	1.7	14	133
33-36.7	11.0	24	260
40-46.8	21.6	35	422

ments, at least for particles above ~ 4 GeV. Therefore, the kinematics of reactions (1) and (2) can be precisely reconstructed from accurate angle measurements. Furthermore, it is possible to take into account the possible radiation of a photon along the incident electron or positron directions and to calculate the energies of the four final state particles.

Such a calculation has been performed on the event sample, resulting in a distribution for radiative photon energy k_{rad} shown in fig. 2: we observe a sharp peak for $k_{\text{rad}} < 0.04 E_{\text{beam}}$ consistent within resolution with reactions (1) and (2), and a radiative tail as expected from initial state radiation. Since radiative events can also be used for the exploration of new phenomena which could occur in reactions (1) and (2), we have retained in our sample events with $k_{\text{rad}} < 0.20 E_{\text{beam}}$.

In order to test the kinematic reconstruction we have made a detailed study of the mass resolutions. From the known resolution of the angles of the photon and the charged particles, we expect a lepton-photon mass resolution, $\sigma_M^{\text{angles}} = 250 \text{ MeV} (E_{\text{beam}}/17 \text{ GeV})$ for a mass of 30 GeV (weakly dependent on the value of the mass). It is also possible to measure

the same mass from the recoil momentum of the second lepton, with a small correction due to initial state radiation: such a determination competes in precision with the previous method only for large masses, where the recoiling lepton has a momentum not exceeding a few GeV/c. For example, a 30 GeV mass is reconstructed using the recoil momentum with a resolution $\sigma_M^{\text{momentum}} = 340 \text{ MeV}$ at $\sqrt{s} = 34 \text{ GeV}$ rising to 2.4 GeV at $\sqrt{s} = 43 \text{ GeV}$. We have two independent checks of the kinematic treatment: (i) the Monte Carlo simulation with known angular resolutions as input predicts correctly the energy resolution (1.3% of the beam energy) of the radiated photon along the beams as demonstrated in fig. 2, and (ii) there is good agreement between the two independent determinations of the lepton-photon mass – from angles or from momentum – in configurations where their precisions are comparable. We have also tried a complete 3C kinematic fit (allowing initial radiation along the beam direction) with no significant improvement in resolution; this is expected since the energy measurements of the fast lepton and the photon bring little additional information at this level of precision. In summary, the analysis tells us that the events satisfy the kinematics of reaction (1) or (2) with the possible emission of an additional photon along the beam line.

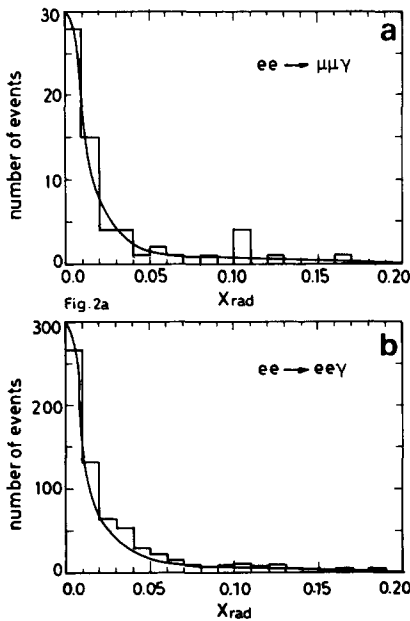


Fig. 2. (a), (b) The distribution of $x_{\text{rad}} = k_{\text{rad}}/E_{\text{beam}}$ for the computed radiative photon along the beam line. The curve is the QED expectation, including experimental resolution and the radiative tail.

Background estimates. Reaction (2) is well identified with the help of the electromagnetic calorimeter and although its rate is typically one order of magnitude larger, its misidentification as reaction (1) is negligible (less than 10^{-3} of the $\mu\mu\gamma$ rate). The contributions from the reactions

$$e^+e^- \rightarrow \tau^+\tau^-\gamma, \tag{3}$$

$$e^+e^- \rightarrow \tau^+\tau^-\gamma, \tag{4}$$

are to a large extent removed by scanning since the final state contains π^0 and hadronic showers for most of the τ decays [7]. The remaining part, which can simulate reaction (1), is considerably reduced after the kinematic constraints are applied, and amounts to at most 2×10^{-2} of the $\mu\mu\gamma$ rate. In the domain defined by $M_{\mu\gamma}^2/s > 0.01$, this contamination falls to a level of less than 6×10^{-3} .

The reaction

$$e^+e^- \rightarrow \pi^+\pi^-\gamma \tag{5}$$

can be recognized by hadronic showers in the calori-

meter. The non-observation of such events allows us to set a purely experimental upper limit of 6×10^{-2} of the observed $\mu\mu\gamma$ rate for reaction (5). An estimate which takes into account the pion form factor gives a maximum possible contamination of 1×10^{-4} .

We have also examined the process where two photons are produced at large angles with respect to the beam

$$e^+e^- \rightarrow \mu^+\mu^-\gamma\gamma. \quad (6)$$

This could simulate $\mu\mu\gamma$ events if one of the two photons escapes detection. If the energy of the observed second photon is larger than 0.5 GeV, we compute [8] a yield of 3.4 events at $\sqrt{s} > 33$ GeV, where we observe 3 events. Taking into account the detection losses and the kinematic fitting, we estimate the contamination to be less than 2×10^{-3} of the $\mu\mu\gamma$ rate. The corresponding reaction with electrons

$$e^+e^- \rightarrow e^+e^-\gamma\gamma \quad (7)$$

also occurs at a similar rate (relative to reaction (2)).

In summary, for the region $M_{\mu\gamma}^2/s > 0.01$ and $M_{\mu\mu}^2/s > 0.01$ discussed below, the total contamination in the $\mu\mu\gamma$ sample is estimated to be less than 9×10^{-3} of the $\mu\mu\gamma$ rate expected from QED, decreasing to 3×10^{-3} at large $\mu\gamma$ masses. The contamination in the $e\gamma$ sample is less than 5×10^{-3} .

Comparison with QED and discussion. A complete description of processes (1) and (2) by QED to order α^3 is available [1,2] and widely used Monte Carlo generators exist. We have used such programs ^{#1} and have also performed an independent Monte Carlo generation of events from reaction (2) which should be valid for hard radiation. We have included initial and final state radiative corrections to order α^4 following the prescription of Tsai [8], and estimate our knowledge of the absolute normalization to be $\pm 10\%$.

All information concerning the reaction $ee \rightarrow \ell\ell\gamma$ for unpolarised beams can be obtained from the Dalitz plot $(M_{\ell\ell}^2, (M_{\ell\gamma}^2)_{\text{low}}, (M_{\ell\gamma}^2)_{\text{high}})$, the orientation of the event plane with respect to the beam axis and the orientation of the event within this plane. We first consider the Dalitz plot population.

Since we are interested in the possibility of new phenomena, cuts are applied in order to eliminate the regions where the QED cross section is largest, name-

ly: $M_{\ell\ell}^2/s > 0.01$ and $M_{\ell\gamma}^2/s > 0.01$. These regions correspond to enhancements in the amplitudes for initial and final state radiation, respectively. Fig. 3 presents the experimental Dalitz plot distributions after these cuts. Since the data are spread over a large energy range, we group the data in three energy domains and use dimensionless variables. Consequently the Dalitz plot population should be energy independent up to an overall normalization factor. It should be emphasized that our kinematic knowledge of the events is such that the uncertainty on the Dalitz plot is very small $\Delta M_{\ell\gamma}^2/s < 0.01$. To compare with QED, 3 regions are defined and their respective population is compared to the corresponding QED predictions in table 2. Estimated background contributions are also included.

Good agreement with QED is observed in all regions except for reaction (1) in region III of figs. 3b and 3c ($\sqrt{s} > 33$ GeV; $(M_{\mu\gamma}^2)_{\text{high}}/s > 0.8$), where we observe 12 events and expect 3.9. In order to assess the overall statistical significance of the observed enhancement independent of the boundary between regions II and III, we directly compared the experimental $\mu\gamma$ mass spectrum to the expected QED distribution in these regions. A Kolmogorov test gives a probability of 1% that the Monte Carlo describes the data. This probability rises to 2%, when the uncertainty in the mass determination is stretched in the direction most favourable to QED.

The lepton-photon mass distributions from regions II and III are shown in fig. 4: no significant structure is observed in either the $\mu\gamma$ or the $e\gamma$ mass distributions.

We have examined other variables besides the invariant masses. Fig. 5 shows the distribution of the photon angle with respect to the e^- beam direction. No deviation from QED is observed. In particular, the events in region III of the Dalitz plot show an angular distribution consistent with initial state radiation (shaded area in fig. 5a).

Previous analyses of reaction (1) have been reported. The data from MAC [9] at $\sqrt{s} = 29$ GeV are in good agreement with QED, like our data in the lower energy range. The analysis performed by MARK J [10] on data taken at \sqrt{s} up to 36.7 GeV indicates no deviation from QED but the cuts differ from ours in such a way that the sensitivity to new phenomena is reduced at large $\mu\gamma$ masses. JADE has recently published [11,12] an analysis of reactions (1) and (2)

^{#1} The Monte Carlo generators were based on refs. [2,4].

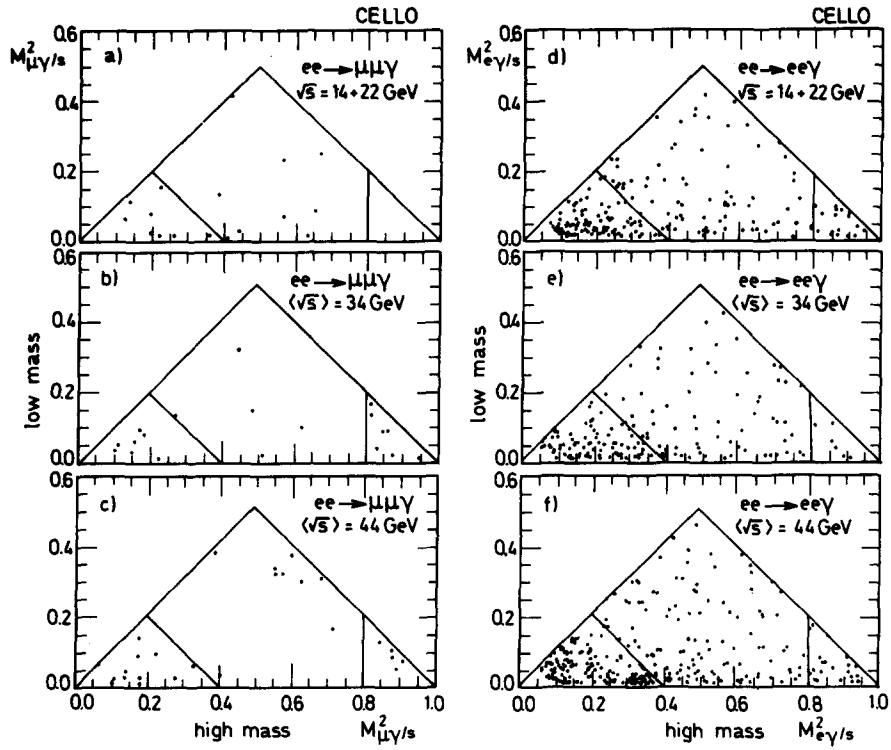


Fig. 3. (a)–(f) The Dalitz plot population for the reactions $e^+e^- \rightarrow \mu^+\mu^-\gamma$ and $e^+e^- \rightarrow e^+e^-\gamma$ in the three different energy regions.

Table 2

Population of the Dalitz plot in 3 regions. Region I: $0.6 < M_{\mu\mu}^2/s < 0.9$. Region II: $M_{\mu\mu}^2/s < 0.6$ and $M_{\mu\gamma}^2/s < 0.8$. Region III: $M_{\mu\gamma}^2/s > 0.8$. In addition $M_{\mu\gamma}^2/s > 0.01$ and $M_{\mu\mu}^2/s > 0.01$.

Reaction	\sqrt{s} (GeV)	Contribution	Region		
			I	II	III
$ee \rightarrow \mu\mu\gamma$	14 +22	data	8	9	0
		MC	7.0	7.4	1.4
		background	<0.1	<0.1	<0.01
	33.1–36.7	data	7	5	7
		MC	8.1	8.7	1.6
		background	<0.1	<0.1	<0.01
	40 –46.8	data	12	9	5
		MC	12.2	12.5	2.3
		background	<0.1	<0.1	<0.01
$ee \rightarrow ee\gamma$	14 +22	data	80	76	17
		MC	90.1	71.4	9.7
		background	<0.1	<0.1	<0.1
	33.0–36.7	data	98	85	8
		MC	99.4	77.9	10.1
		background	<0.1	<0.1	<0.1
	40 –46.8	data	144	124	22
		MC	161.2	126.4	16.3
		background	<0.1	<0.1	<0.1

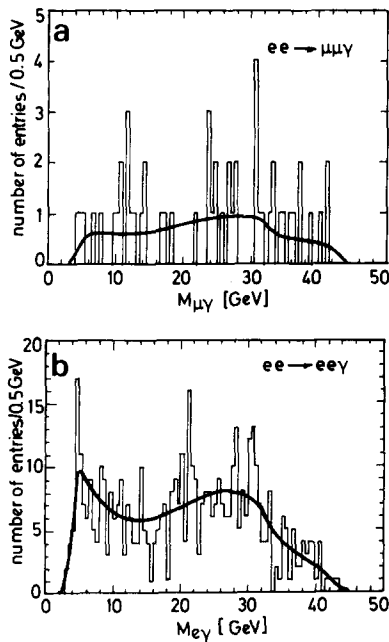


Fig. 4. (a), (b) The distribution of the lepton-photon invariant masses for $\sqrt{s} > 33$ GeV corresponding to regions II + III in fig. 3. The curves are the prediction from the QED Monte Carlo calculations.

using again data at \sqrt{s} up to 36.7 GeV for $M_{\mu\gamma} > 30$ GeV and found good agreement with QED.

In conclusion, we have measured the properties of the radiative processes $ee \rightarrow \mu\mu\gamma$ and $ee\gamma$. We find that QED provides a proper description of our data, except for an excess of events for $\sqrt{s} > 33$ GeV and $M_{\mu\gamma}^2/s > 0.8$. The probability that this excess is due to a statistical fluctuation is at the 10^{-2} level.

We gratefully acknowledge the outstanding efforts of the PETRA machine group which made possible these measurements. We are indebted to the DESY computer center for their excellent support during the experiment. We acknowledge the invaluable effort of the many engineers and technicians from the collaborating institutions in the construction and maintenance of the apparatus, in particular the operation of the magnet system by M. Clausen and the cryogenics group. The visiting groups wish to thank the DESY directorate for the support and kind hospitality extended to them. This work was partly supported by the Bundesministerium für Forschung und Technologie (Germany), by the Commissariat à l'En-

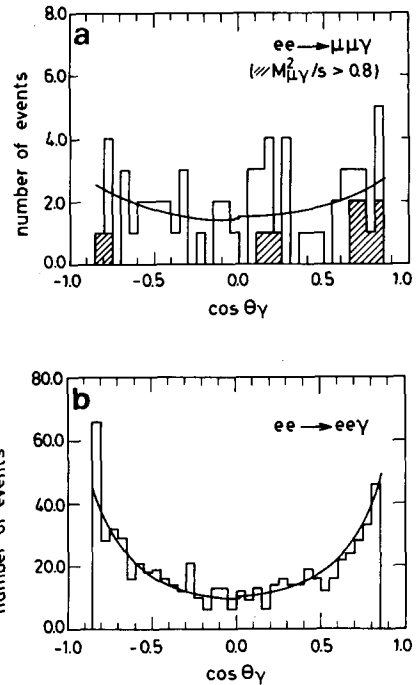


Fig. 5. (a), (b) The distribution of the $\cos \theta$ of the photon with respect to the e^- beam direction compared to the QED Monte Carlo prediction.

ergie Atomique and the Institut National de Physique Nucléaire et de Physique des Particules (France), by the Science and Engineering Research Council (UK), and by the Israeli Ministry of Science and Development.

- [1] F. Berends, K. Gaemers and R. Gastmans, Nucl. Phys. B57 (1973) 381; B63 (1973) 381; F. Berends and R. Kleiss, Nucl. Phys. B177 (1981) 237.
- [2] F. Berends, R. Kleiss and S. Jadach, Nucl. Phys. B202 (1982) 63.
- [3] F. Berends, K. Gaemers and R. Gastmans, Nucl. Phys. B68 (1974) 541.
- [4] F. Berends and R. Kleiss, Nucl. Phys. B228 (1983) 573.
- [5] CELLO Collab., H.-J. Behrend et al., DESY 84-101 (October 1984).
- [6] CELLO Collab., H.-J. Behrend et al., Phys. Scripta 23 (1981) 610.
- [7] CELLO Collab., H.-J. Behrend et al., Phys. Lett. 114B (1982) 282; 127B (1983) 27.
- [8] Y.S. Tsai, SLAC-Pub 3129 (1983).
- [9] MAC Collab., W.T. Ford et al., Phys. Rev. Lett. 51 (1983) 257.
- [10] MARK J Collab., B. Adeva et al., Phys. Rev. Lett. 48 (1982) 967.
- [11] JADE Collab., W. Bartel et al., Z. Phys. C24 (1984) 223.
- [12] JADE Collab., W. Bartel et al., Z. Phys. C19 (1983) 197.